10208 *Biochemistry* **2009,** *48,* 10208–10219
DOI: 10.1021/bi901433n

BIOCHEMISTRY
including biophysical chemistry & molecular biology
Article

Solution Structure and Functional Characterization of Human Plasminogen Kringle 5[†,‡]

Marcos D. Battistel,[§] Alexander Grishaev,[§,∥] Seong Soo A. An,[§,⊥] Francis J. Castellino,[#] and Miguel Llinás*[,§]

[§]*Department of Chemistry, Carnegie Mellon University, 4400 Fifth Avenue, Pittsburgh, Pennsylvania 15213, and* [#]*W. M. Keck Center for Transgene Research, University of Notre Dame, Notre Dame, Indiana 46556* [∥]*Current address: National Institute of Diabetes and Digestive and Kidney Diseases, NIH, Bethesda, MD 20892-2560* [⊥]*Current address: College of Bionano Technology, Kyungwon University, Gyeonggi-do 461-701, Korea*

Received April 15, 2009; Revised Manuscript Received August 24, 2009

ABSTRACT: The ligand binding properties of the kringle 5 (K5) domain of human plasminogen have been investigated via intrinsic tryptophan fluorescence. The oleic acid (OA) affinity for K5 was quantified, yielding an association constant $K_a \sim 2.08 \times 10^4$ mM^{-1}. Simultaneously, it was determined that OA and *trans*-4-(aminomethyl)cyclohexanecarboxylic acid (AMCHA) ($K_a \sim 50$ mM^{-1}) compete for binding to K5. The solution structure of K5 in the presence of 11 mM AMCHA was solved via NMR spectroscopy (protein heavy atom RMSD $\sim 0.93 \pm 0.12$ Å). The AMCHA binding site was localized via $^1H/^{15}N$ chemical shift perturbation mapping assisted by *in silico* docking. We have found that AMCHA binds at the canonical kringle lysine binding site (LBS), structured by the Pro54−Gly60 segment plus the neighboring Phe36, Thr37, Trp62, Leu71, and Tyr72 residues. The segment 30−42, encompassing LBS residues, appears to be endowed with a higher degree of structural flexibility as suggested by the relatively lower value of S^2, the generalized order parameter, consistent with a higher backbone heavy atom RMSD of ∼1.22 Å (vs 0.84 Å overall) between the two monomeric units in the crystal unit cell, of potential significance for ligand binding. OA was found to perturb the same area of the protein, namely, the LBS, as well as Tyr74. Combined with previous studies, the observation of OA binding expands the range of ligands that interact with kringle 5 while it widens the scope of potential biological functions for kringle domains.

Plasminogen (Pgn)[1] is the inactive proenzyme of plasmin (Plm), a blood plasma proteinase involved in fibrinolysis, extracellular matrix degradation, tissue remodeling, metastasis, and other roles of clinical relevance. Pgn is composed of a sequence of 791 amino acid residues. The protein is structured as an in-tandem array of seven globular domains (*1*, *2*): a preactivation N-terminal peptide (residues 1−76), five kringle repeats (K) (77−561), and a trypsin-like serine protease zymogen, responsible for the proteolytic activity of Plm (562−791) (*1*−*3*).

Kringles are triple-looped structures of ca. 80 amino acids each, constrained by a characteristic, strictly conserved, three-cystine bridge pattern: Cys1−Cys6, Cys2−Cys4, and Cys3−Cys5, where the proximal Cys2−Cys4 and Cys3−Cys5 S−S bonds cross each other providing a signature of the kringle fold (*3*, *4*). Despite their rather uniform structural characteristics, kringles display a variety of ligand specificities (*5*). Thus, while the human Pgn (HPgn) K1 and K4 show preference for lysine-like dipolar molecules, K2 and K5 display marginal affinity for these types of ligands with K3 not interacting measurably with such zwitterions.

It has been reported that long-chain fatty acids (LCFA) inhibit Plm activity (*6*−*8*), which would affect Pgn activation (*9*). Moreover, it has been postulated that the modulation of Plm activity by LCFA is mediated by lysine binding sites (LBSs) in Plm (*6*−*8*). Recently, Huet et al. have investigated various kringle-containing HPgn fragments and proposed, from surface plasmon resonance experiments, that K5 (Scheme 1) exhibits the highest affinity for OA (*8*). However, to date no direct evidence has been reported identifying, at the molecular level, the mechanism by which K5 is involved in the interaction.

The affinity of the human Pgn K5 toward lysine-like zwitterions is rather weak ($K_a < 11$ mM^{-1}) except for AMCHA (Scheme 2), a cyclic analogue of lysine ($K_a \sim 44$ mM^{-1}) (*5*). The X-ray crystallographic structure of the ligand-free K5 at 1.7 Å resolution has been published (*10*). Here, we report on the NMR solution structure of the K5 domain in the presence of AMCHA, its dynamics properties, the K5 interaction with OA and on the contact surface for both ligands (Scheme 2).

MATERIALS AND METHODS

Ligand Binding Titration Experiments by Fluorescence. Wild-type K5 was generated via pepsin hydrolysis of miniplasminogen as previously reported (*11*). In order to boost the yield

[†]This research was supported by National Institutes of Health Grants HL029409 (to M.L.) and HL013423 (to F.J.C.).

[‡]Coordinates for the ensemble of 20 K5 NMR structures (2KNF) have been deposited in the RCSB Protein Data Bank. Experimental NMR restraints and ^1H and ^{15}N chemical shift assignments (16466) have been deposited in the Biological Magnetic Resonance Bank.

*Corresponding author: e-mail, llinas@andrew.cmu.edu; telephone, 412-268-3140; fax, 412-268-6897.

[1]Abbreviations: AMCHA, *trans*-4-(aminomethyl)cyclohexanecarboxylic acid; COSY, 2D correlation spectroscopy; DQF-COSY, double-quantum-filtered COSY; dss, sodium 2,2-dimethyl-2-silapentane-5-sulfonate; HPgn, human Pgn; K, kringle domain; K_a, association binding constant; K_d, dissociation constant; K1, kringle 1; K2, kringle 2; K3, kringle 3; K4, kringle 4; K5, kringle 5; LBS, lysine binding site; LCFA, long-chain fatty acid; LGA, Lamarckian genetic algorithm; NMR, nuclear magnetic resonance; NOE, nuclear Overhauser effect; NOESY, 2D NOE spectroscopy; OA, oleic acid; PDB, Protein Data Bank; Pgn, plasminogen; pH*, pH electrode reading, uncorrected for isotope effects; PLA_2, phospholipase A_2; Plm, plasmin; RMSD, root mean square deviation; $R_1 = (T_1)^{-1}$; $R_2 = (T_2)^{-1}$; SOS, sucrose octasulfate; S^2, generalized order parameter; TOCSY, 2D total correlation spectroscopy; tPA, tissue-type plasminogen activator; T_1 and T_2, longitudinal and transverse relaxation times; uPA, urokinase-type plasminogen activator; xNOE, $^1H/^{15}N$ heteronuclear NOE; 1D, 2D, and 3D, one, two, and three dimensional, respectively.

 Published on Web 08/26/2009

Scheme 1: Outline of the Kringle 5 Primary Structure[a]

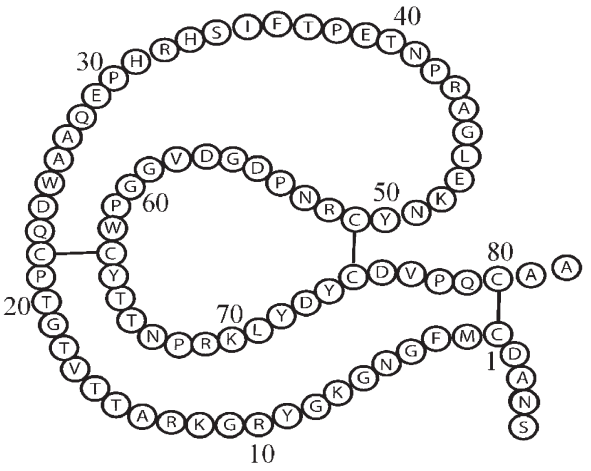

[a]Amino acid residues are labeled according to the conventional one-letter code and numbered starting at the first half-cystine.

of K5, the protein was saturated with AMCHA as the ligand decreases its aggregation and tendency to precipitation (*12*). Recombinant, uniformly ^{15}N-labeled K5 was obtained from the laboratory of F. J. Castellino (*13*), by reference to the K5 construct comprising sequence 456−542 of HPgn.

Fluorescence quenching experiments were performed using a Photon Technology International (PTI, Birmingham, NJ) instrument. Intrinsic fluorescence was measured by irradiating at 295 nm for selective tryptophan excitation, using a 75 W xenon lamp. A 3 mm path length quartz cuvette (Starna) was used for all fluorescence experiments. Emission spectra were collected from 315 to 350 nm in steps of 0.5 nm with integration time set at 0.5 s. The bandwidth for both excitation and emission monochromators was 5 nm. Changes in tryptophan fluorescence upon addition of ligand solution were measured at 298 K.

For ligand titrations, the protein was dissolved to a final concentration of 5 μM in either 50 mM sodium phosphate (pH 7.2) or 50 mM sodium acetate (pH 5.1), both containing 0.05% NaN_3. For the fluorescence quenching assays, aliquots of 0.25 μL of concentrated solutions of either AMCHA or OA (Sigma-Aldrich) were added to a 5 μM solution of K5. After each ligand addition the system was allowed to equilibrate until no change in fluorescence was observed; three emission spectra were recorded and averaged. A blank titration was performed to correct for volume effects and for fluorescence changes resulting from the addition of an ethanolic solution of OA. Competition binding experiments were carried out on K5 dissolved in the phosphate buffer in the presence of a 10-fold molar excess of AMCHA.

We define $[K_0]$, [S], and [KS] as the total kringle, the equilibrium substrate, and the kringle−substrate complex concentrations, respectively. Δp is the fraction of ligand-bound kringle, at equilibrium, to the total kringle concentration. Namely

$$\Delta p = \frac{[KS]}{[K_0]} = \frac{F_{obs} - F_{free}}{F_{bound} - F_{free}} \quad (1a)$$

where $F_{obs} - F_{free}$ is the fluorescence intensity change measured at each ligand titration point and $F_{bound} - F_{free}$ is the maximum change in fluorescence intensity as detected at ligand close to saturation. It follows (*5*) that K_a, the equilibrium ligand−kringle association constant, can be estimated from the experimentally determined Δp

Scheme 2: Chemical Structures and Estimated Molecular Lengths of the Two Investigated Ligands

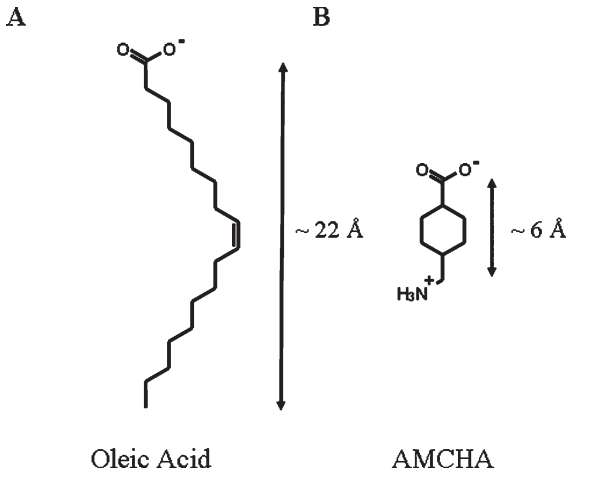

$$\Delta p = \frac{PK_a[S]}{1 + K_a[S]} \quad (1b)$$

by iteratively fitting K_a and the normalization parameter P to eq 1b until convergence (P = 1). Fluorescence changes were measured as differences of integrated emission spectra.

Circular Dichroism Analysis of HPgn K5. CD measurements were performed on a Jasco-715 spectropolarimeter equipped with a PFD 350S Peltier-type temperature controller. CD spectra (260−185 nm) were recorded at 298 K at a protein concentration of 10 μM (in H_2O), pH 5.1, using a 0.1 cm path length quartz cell (Starna). From the CD spectra, secondary structure prediction was carried out via the SELCON3, CDSSTR, and CONTIN programs within the CDPro software package (*14*).

NMR Spectroscopy. Samples of K5 or ^{15}N-labeled recombinant kringle 5 (^{15}N-K5) were dialyzed against water at pH 3 in order to exclude potential ligands remaining from the K5 purification procedure (*15*) and lyophilized. The protein was further purified using a G-50 Sephadex column and lyophilized. Protein purity was assessed by HPLC and MALDI-TOF-MS. The measured mass, 9550 ± 5 Da, was in close agreement with that expected for the construct Ser-Asn-Ala-Asp-K5-Ala-Ala (theoretical 9557 Da), where K5 corresponds to the 456−542 segment of (^{15}N) HPgn.

(A) NMR Sample Preparation for Structure Determination. ^{15}N-K5 was dissolved in 300 μL of 50 mM phosphate, pH* 5.1, 0.02% NaN_3, and 10% ^2H_2O to a final concentration of 2.2 mM and 11 mM AMCHA. Under ligand presence the spectrum shows improved signal/noise (*11*) as the K5 solubility is enhanced and the protein is less prone to aggregation as evidenced by narrower NMR resonance signals and T_1/T_2 relaxation criteria. Consistent with a folded, native kringle structure, the ^{1}H NMR spectrum of K5 exhibited the characteristic ∼5−12 ppm spread of aromatic resonances, as well as the "fingerprint" methyl H^δ doublets at −1.085 and 0.36 ppm arising from of the strictly conserved Leu46 residue[2] (*11*).

NMR spectra were acquired using a Bruker DRX 500 MHz (11.1 T) spectrometer at 298 K. Data processing was carried out with NMRPipe (*16*) and analyzed using the CcpNmr Analysis software package (*17*). Chemical shifts, deposited in BMRB (accession code 16466), are reported by reference to

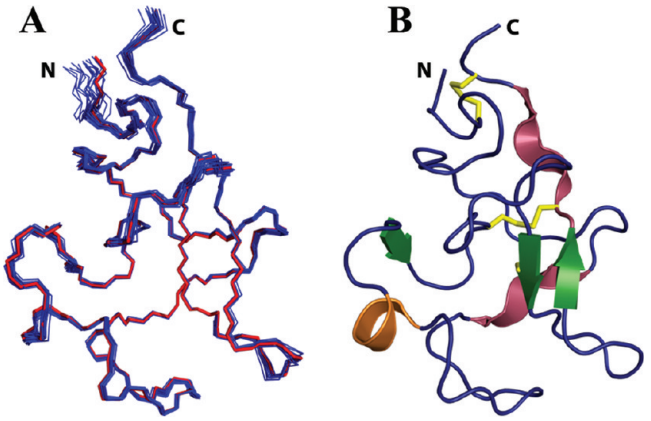

FIGURE 1: NMR structure of Pgn kringle 5. (A) 20 superposed computed backbone traces of segment −4 to 82. The red trace corresponds to the backbone heavy atoms of the closest-to-the-mean structure. (B) Secondary structure of the closest-to-the-mean fold. β-Strands are represented by green arrows, 3_1 helices are in purple, and the α-helical turn is in orange. Cystine bridges are depicted in yellow.

external dss using *p*-dioxane as an internal standard (δ 3.75 ppm) (*18*); ^{15}N chemical shifts were derived accordingly (*19*).

Proton resonances were partially assigned from homonuclear COSY, DQF-COSY, NOESY, and TOCSY experiments on ^{14}N-protein samples. The assignments were substantiated and completed via ^{1}H/^{15}N-HSQC, ^{15}N-edited TOCSY, and NOESY (at 100, 150, and 200 ms mixing times) experiments, which also yielded the ^{15}N assignments. All expected polypeptide backbone and 88.2% of the ^{1}H/^{15}N side-chain resonances were assigned. The $^{3}J_{H^{\alpha}-H^{N}}$ coupling constants were estimated from an HNHA experiment (*20*). These were interpreted in terms of compatible ϕ dihedral angles.

(*B*) *Deuterium Exchange Experiments*. The K5 backbone amide ^{1}H−^{2}H exchange, both ligand-free and in the presence of AMCHA, was monitored via ^{15}N/^{1}H-HSQC spectra at 298 K, acquired at incremental time intervals, up to 72 h after dissolving the sample in $^{2}H_2O$, pH* 5.1 (50 mM phosphate buffer, 0.02% NaN_3).

Structure Calculation. NOEs were extracted from the 2D and 3D NOESY by combining data from the various mixing times. After removing symmetry-related and diagonal peaks, 1002 2D homonuclear and 1616 3D heteronuclear NOE cross-peak intensities were obtained. Assigned NOEs were converted to flat-bottom interproton distances ranging within 1.8−5.0 Å. For structure calculations of the HPgn K5−AMCHA complex in the presence of AMCHA, 1604 intrakringle nonredundant NOE-derived interproton distances along with 54 backbone ϕ dihedral angles were used as restraints. Among the distance restraints, 222 were intraresidue, 476 sequential, 320 medium range ($2 \leq |i - j| \leq 4$), and 586 long range ($|i - j| \geq 5$). Restraints for 54 backbone ϕ angles were derived from the experimental $^{3}J_{H^{\alpha}}-H^{N}$ splittings estimated from an HNHA experiment (*20*).

The K5 structure (Figure 1) was obtained via a Cartesian molecular dynamics simulated annealing protocol with temperature linearly ramped from 10000 to 0 K under active interproton distance and backbone dihedral angle restraints. A repulsive-only quadratic energy term was used to represent the nonbonded interactions with atomic radii scaled down by 0.8. In the first stage, an initial fold was generated from 100 randomized coordinates using unambiguously assignable NOE and ϕ restraints, devoid of disulfide linkages to improve convergence. Twenty structures with lowest restraint violations were selected for the subsequent refinement cycles in which the three disulfides were reintroduced, first with S−S distance restraints and subsequently including all appropriate empirical energy terms. In the following two stages of refinement, interproton distance restraints were assigned automatically using BACUS (*21*). Afterward, NOE cross-peak assignments were updated after each cycle, taking into account the resulting structural models at given stages (*22*, *23*), with up to 9 rounds of refinement. Subsequent rounds of structure calculation included 712 uniquely assignable distance restraints from 2D NOESY and 1150 restraints from 3D NOESY. Peaks that had multiple possible assignments, 95 from 2D NOESY and 331 from 3D NOESY, were not converted to restraints for structure calculation. At the later stages of refinement, 22 backbone−backbone hydrogen bonds were identified based on the $O\cdots H^{N}$ distance (below 3.0 Å) and $C-O\cdots H^{N}$ and $N-H^{N}\cdots O$ (above 100°) angular criteria and enforced via a previously described database potential of mean force (*24*). On the same basis, 27 additional backbone−side-chain hydrogen bonds were identified and enforced as pairwise distance restraints.

The final bundle was calculated by inputting the above restraints into Aria 2.2 (*25*). After removing redundant and nonrestrictive restraints via AQUA (*26*−*28*), a total of 1604 unambiguous NOE-derived distance restraints, combined from 2D and 3D NOESY data, were used (Table 1). From 100 generated structures, 20 were selected for the final bundle, on the basis of their total energy value and Ramachandran plot characteristics.

The statistical analysis was carried out on the selected ensemble of 20 water-refined structures (Table 1 and Figure 2A) (PDB ID 2KNF). For the K5 proper, as defined by the folded Cys1−Cys80 sequence, the mean RMSD values for backbone + side-chain heavy atoms and polypeptide backbone heavy atoms are 0.93 ± 0.12 and 0.33 ± 0.07 Å, respectively.

Analysis of the HPgn K5 secondary structure, independently assessed via CD spectroscopy, was aided by use of software packages WHATIF (*29*), STRIDE (*30*), and XTLSSTR (*31*).

HPgn K5 Polypeptide Backbone Dynamics. Relaxation data were collected for the recombinant K5 in the presence of AMCHA. Backbone ^{15}N T_1 and T_2, as well as steady-state heteronuclear ^{1}H/^{15}N NOE were measured on a Bruker-DRX 500 (11.7 T) at 298 K using, with minor modifications, the pulse sequences of Farrow et al. (*32*) and Grzesiek and Bax (*33*). The T_1 and T_2 relaxation data were calculated for well-resolved resonances via a nonlinear least-squares fit (nlinLS) implemented in NMRPipe (*16*). Heteronuclear NOE (xNOE) values were extracted as a ratio of peak intensities with/without proton saturation. Relaxation data were analyzed following the model-free approach (*34*, *35*) using Fast Model-Free (*36*) and Model-Free (v.4.2) software (*34*−*36*). The effective isotropic rotation correlation time, τ_c, was estimated from the 10% trimmed average of T_1/T_2 ratio (*37*). Five models were tested against the experimental data optimizing the following free parameters: (i) generalized order parameter S^2, (ii) S^2 and the internal time scale parameter τ_e, (iii) S^2 and the chemical exchange parameter R_{ex}, (iv) S^2, τ_e (fast time scale), and R_{ex}, and (v) S^2, τ_e (slow time scale), and order parameter for internal motion on fast time scale $S_f{}^2$.

Characterization of AMCHA and Oleic Acid Binding to K5 by NMR. ^{15}N-HSQC NMR ligand titration experiments were performed in order to estimate affinities of the various ligands for K5. Small aliquots of ligand solution were sequentially added to the protein solution at pH* 5.1, 298 K. For each titration point, 256 transients with a ^{1}H spectral width of 8012 Hz

Table 1

restraints	
distances	
total	1604
intraresidue $(i-j)=0$	222
interresidue sequential $(i-j)=1$	476
interresidue medium range $5>(i-j)>1$	320
interresidue long range $(i-j)>4$	586
Φ dihedral angle	54
hydrogen bonds	
total	49
backbone−backbone	22
backbone−side chain	27

structure statistics[a]

	ensemble	selected structure[b]
av RMSD from exptl restraints		
distance restraint (Å)	0.05 ± 0.01	0.05
dihedral restraint (deg)	1.90 ± 0.09	1.87
RMSD from idealized covalent geometry[c]		
bonds (Å)	0.0063 ± 0.0001	0.0066
angles (deg)	0.66 ± 0.02	0.70
impropers (deg)	1.96 ± 0.08	2.13
coordinates av RMSD (Å)[d]		
side-chain + backbone heavy atoms		
all	0.95 ± 0.11	0.61
residues 1−80	0.93 ± 0.12	0.61
backbone heavy atoms		
all	0.43 ± 0.08	0.25
residues 1−80	0.33 ± 0.07	0.21
mean energy (kcal/mol)		
bond	52 ± 2	50
angle	154 ± 8	151
impropers	421 ± 33	444
dihedral	417 ± 4	420
VDW	−769 ± 37	−748
electrostatic	−3219 ± 47	−3190
total	−2944 ± 85	−2898
Ramachandran plot (% content)		
core	69.0	67.2
allowed	29.6	31.3
generously allowed	0.2	0
disallowed	1.3	1.5

[a]Restraints utilized for structure calculation and statistical analysis performed over a bundle of the 20 lowest Ramachandran map energy structures. [b]Closest to the mean (Figure 1). [c]Idealized covalent geometry based on the Aria 2.2 parallhdg5.0.pro force field (*25*). [d]Obtained by averaging coordinates of the 20 calculated structures, superposed using polypeptide N, C^{α}, and C′ atoms.

were combined; higher resolution experiments (512 F2-spectra) were collected at the beginning, middle, and end of the titration experiments. Spectra acquired under excess ligand conditions were assigned and compared to the ligand-free spectrum (*38*, *39*). Differences in chemical shifts were expressed in terms of $\Delta\delta$ for the ^{1}H and ^{15}N chemical shifts on the basis of (*40*)

$$\Delta\boldsymbol{\delta} = \sqrt{(\Delta\boldsymbol{\delta}^{1}\mathrm{H} \times 500)^2 + (\Delta\boldsymbol{\delta}^{15}\mathrm{N} \times 50.7)^2} \qquad (2)$$

where $\Delta\delta^{1}H$ and $\Delta\delta^{15}N$ are the chemical shift perturbations for proton and nitrogen, respectively. The $\Delta\delta$ values were used to map the binding of AMCHA and OA on the K5 surface.

Analysis of binding site surface and ligand docking was carried out on the NMR solution structure (≡closest to the mean).

Binding Site Analysis. AMCHA and oleic acid (OA) docking on the HPgn K5 structure was predicted via AutoDock4.0 (*41*−*43*). Ligand structures, created via ACD/Laboratories 8.0 sofware

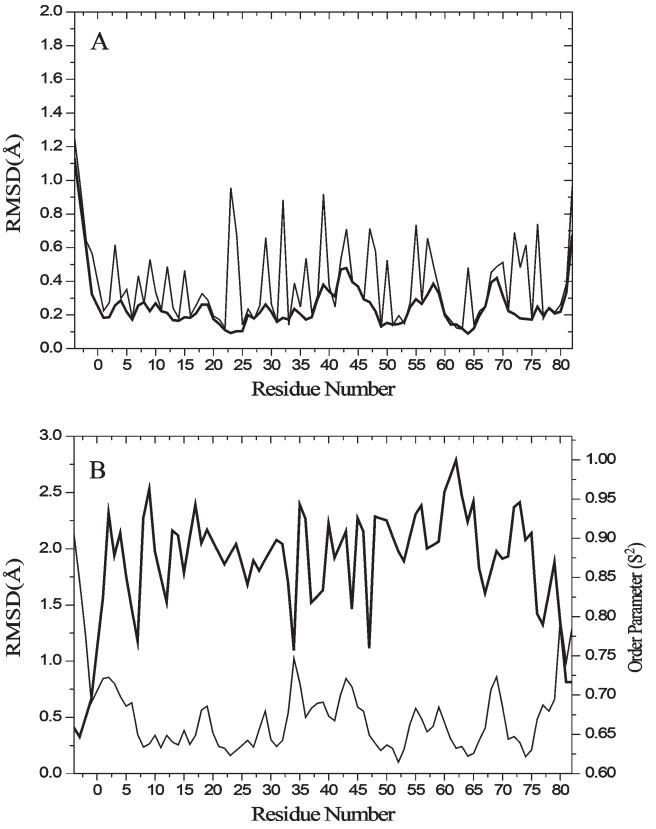

FIGURE 2: Kringle 5 NMR solution structure: RMSD and order parameter. (A) Backbone (N, C^{α}, and C′) (—) and side chain plus backbone (—) bundle averaged heavy atom RMSDs to the mean. The RMSDs were calculated for the ensemble of 20 K5 NMR structures. (B) Inverse correlation between the dynamic derived S^2 (—) and the averaged RMSD (—) between the NMR structure and each of the two X-ray structures.

(Advanced Chemistry Development Inc., Toronto, Ontario, Canada), were used as input for AutoDock Tools v.1.4.5 graphical interface.[2] Unless otherwise specified, the NMR structure of K5 was kept rigid for the docking simulations, using default AutoDock4.0 parameters. For conformational search, the Lamarckian genetic algorithm (L-GA) was utilized as it proves to be robust in terms of effectiveness and reliability (*42*). For each ligand, a total of 10 independent simulations were performed, each run comprising 256 L-GA runs with a population size of 300 individuals. After preliminary trials, a grid with a spacing of 0.353 Å was generated encompassing the LBS of K5 (centered at $x = -5.841$ Å, $y = 0.735$ Å, $z = 17.846$ Å), with box dimensions 62 × 74 × 100 points (~22 × 26 × 35 Å) when treating the protein as rigid (Supporting Information Figure S1A) and 102 × 60 × 100 points (~36 × 21 × 35 Å) when considering residue Arg32 as flexible (Supporting Information Figure S1B). Box dimensions and positioning were optimized based on the experimental NMR chemical shift perturbation data.

To validate the protocol, the same grid and parameters used for the K5−AMCHA docking were applied on the Pgn K2 NMR structure (PDB ID 1B2I) (*44*), originally solved as an AMCHA-complex. The minimum energy AutoDock-obtained AMCHA structure exhibited 0.34 Å RMSD relative to the AMCHA structure as shown in the closest to the mean NOE-derived AMCHA−K2 (*44*). For comparison, the RMSD of the reported

[2]http://mgltools.scripps.edu.

Scheme 3: Exchange-Labile H^N Atoms Remaining at 9 or 72 h after Dissolving the K5 in ^2H_2O, pH* 5 1, 298 K, 2.2 mM Protein Concentration[a]

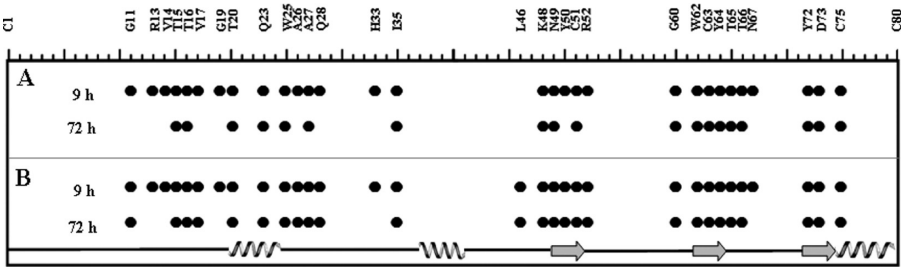

[a]Data recorded from $^1H^{15}N$-HSQC spectra. Kringle 5: (A) ligand-free; (B) in the presence of AMCHA, [AMCHA]/[K5] = 5:1. K5 secondary structares as a function of residue number is shown: β-Strands are depicted as arrows, α-helical turn as right-handed helix, and 3_1-helices as left-handed helices.

20 AMCHA NMR-docked structures is 0.51 ± 0.40 Å; thus, the AutoDock-derived ligand structure falls within the standard deviation of the NMR ensemble.

RESULTS AND DISCUSSION

Kringle 5 Structure. The K5 solution conformation (Figure 1A) reveals the characteristic (*10*, *23*, *44*−*47*) triple-loop kringle fold, in which the two inner cysteine bridges are adjacent and quasi perpendicular to each other. The secondary structure content is ∼22% β-strand (amino acid residues 62−64 and 72−74 and residues 49−51), ∼12% 3_1 helix (residues 20−24 and 75−80), ∼5% α-helix (residues 37−41), and ∼24% β-turn (*29*−*31*) (Figure 1B and Scheme 3). The latter is in close agreement with those predicted (*14*) from analysis of the UV-CD spectrum (Supporting Information Figure S2) as well as by the X-ray crystallographic model (*10*) that yield, approximately, 22% β-strand (X-ray 21%), 13% 3_1 helix (X-ray 13%), 14% β-turn (X-ray 27%), and 2% α-helix (X-ray 5%). The presence of a left-handed, not H-bonded, 3_1 helix is a recurrent feature of the kringle fold (*23*, *44*). CD spectra collected in the presence of excess concentrations of AMCHA and OA are comparable, consistent with no significant secondary structure change upon ligand binding (data not shown). However, AMCHA binding has a stabilizing effect on the K5 structure, as evidenced by retarded $^1H-^2H$ exchange kinetics (Scheme 3, panel B).

Protein Dynamics of the Kringle 5-AMCHA Complex. For the K5−AMCHA complex, 67 backbone resonances were analyzed for the segmental dynamics (9 residues are prolines, hence undetected via $^1H/^{15}N$-HSQC experiments). Longitudinal (T_1) and transverse (T_2) NMR relaxation rates and $^1H/^{15}N$ steady-state NOE (xNOE) experiments were measured. The determined T_1 and T_2, as well as the xNOE, within the Cys1−Cys80 link, averaged to 0.49 ± 0.03 s, 0.11 ± 0.02 s, and 0.75 ± 0.04, respectively. Moreover, excluding the N- and C- termini, K5 exhibits a uniform T_1/T_2 ratio (4.7 ± 0.5), consistent with isotropic rotational diffusion. Estimation of the rotational correlation time (τ_c) from the 10% trimmed average of T_1/T_2 ratio (*37*) yielded $\tau_c \sim 7.2$ ns at 298 K, similar to the value reported for the urokinase kringle (*48*) (7.97 ns) and for the K_{IV} type 8 kringle module of apolipoprotein A (7.23 ns) (*49*), and somewhat higher than the values previously reported for HPgn K1 complexed to ε-ACA (4.2 ns) (*13*) and for the HPgn K2−AMCHA complex (4.5 ns) (*44*), measured at 310 K. The resulting τ_c is somewhat high for a globular protein of ca. 9.5 kDa (*50*) and suggests equilibrium between monomeric and dimeric states. The fact that the crystal of K5 shows a dimer in the unit cell, in which Arg32 of one molecule partially occupies the LBS of the paired molecule (*10*), is consistent with presence of a dimeric form in solution, which would increase τ_c. Furthermore, estimates of τ_c from K5 relaxation data in the absence of ligand (data not shown) yield ∼17 ns compared to 7.2 ns for K5 in the presence of AMCHA. Assuming a globular shape for apo-K5 in H_2O at 298 K, this τ_c value would correspond to a protein of ∼23700 Da rather than 9500 Da expected from the sequence: this indicates ∼2.5 K5 molecules in the multimer. Additionally, the presence of AMCHA improves the appearance of the NMR spectrum, consistent with a disruption of kringle−kringle interactions, leading to lower τ_c and

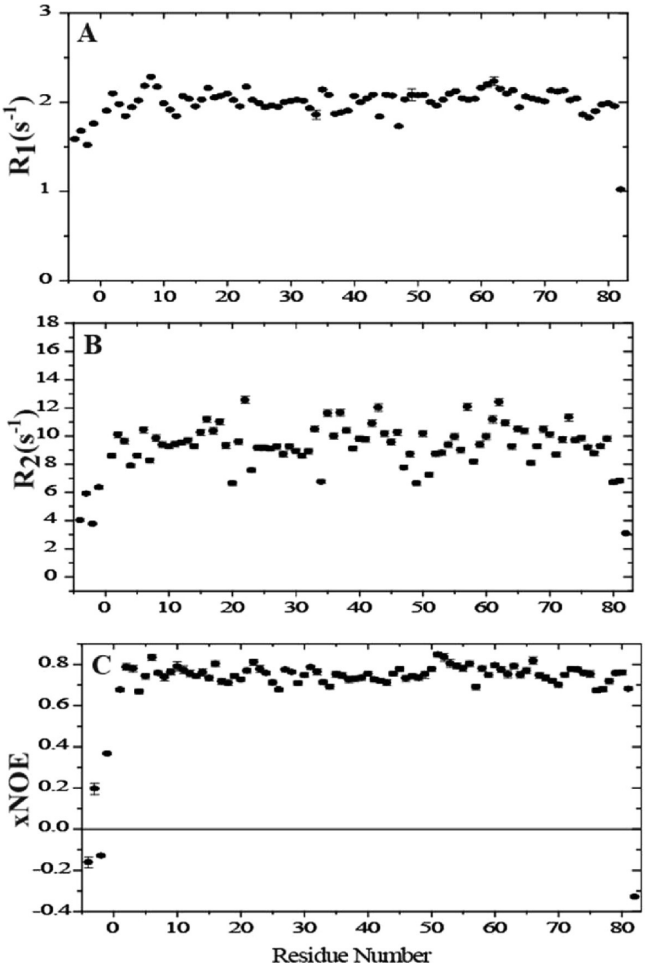

FIGURE 3: Kringle 5 backbone amide NMR relaxation data. (A) $R_1 = (T_1)^{-1}$, (B) $R_2 = (T_2)^{-1}$, (C) $^1H-^{15}N$ xNOE. For residues whose magnetic relaxation could not be monitored (such as prolines), the average between the preceding and following residues' data is reported.

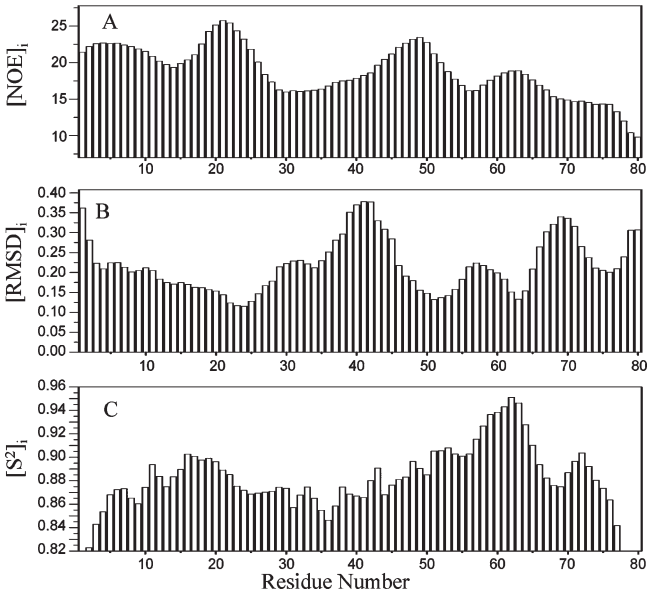

FIGURE 4: Average values of NOE, RMSD, and S^2 for each kringle 5 residue. The data are plotted as histograms against the residue number (i) along the amino acid sequence. The data were convolved with a square window encompassing from residue $i-3$ to residue $i+3$ such that, for each residue i, the reported values $[NOE]_i$, $[RMSD]_i$, and $[S^2]_i$ represent an average over seven sequential residues.

narrower resonance signals with concomitant increased signal/noise. Results are summarized in Figure 3.

In order to account for protein regions with a higher degree of structural disorder, a histogram was constructed, plotting NOEs (i.e., the amount of distance restraints) as a function of protein sequence (Figure 4A). We denote by $[NOE]_i$ the average number of NOEs per residue at the site i, calculated by convolving over a sliding square window spanning segments of seven residues ($i \pm 3$) within the segment. The resulting histogram (Figure 4A) shows maxima at stretches 14−26, 43−54, and 58−67. The first two segments are separated by a region with a lower $[NOE]_i$ (residues 27−42), consistent with a higher degree of structural disorder. A similar square window convolution of the structural RMSD values for the backbone yields the histogram shown in Figure 4B. Two local maxima can be observed between residues 26−47, which inversely correlate with $[NOE]_i$ for the same stretch (Figure 4A). Additionally, when S^2 values are convolved in the same manner as for the NOEs and backbone RMSDs (Figure 4C), the histogram exhibits a wide trough (with lower average $[S^2]_i$) spanning, approximately, residues 25−50. This affords evidence of areas endowed with an extent of disorder in the solution state that are consistent with low $[NOE]_i$ and increased structural $[RMSD]_i$ values. Interestingly, residues that display restricted mobility are those in the short β-sheets (Trp62−Tyr64 with $S^2 = 0.96 \pm 0.04$ and Tyr72−Tyr74 with $S^2 = 0.93 \pm 0.03$). Consistent with this analysis, β-sheet residues also exhibit retarded peptidyl amide $^1H-^2H$ exchange rates (Scheme 3).

In previous studies (*10*−*12*, *51*), segments His33−Thr37, Pro54−Val58, Pro61−Tyr64, and Leu71−Tyr74 were identified as conforming the structure of the K5 putative LBS. By reference to Figure 4, it is apparent that the His33−Thr37 segment coincides with a minimum in the $[S^2]_i$ profile that suggests a higher degree of flexibility for the 30−42 backbone segment, centered at residue 36. It is interesting to note that, in the X-ray crystallographic structure (*10*), segment 30−42 differs between

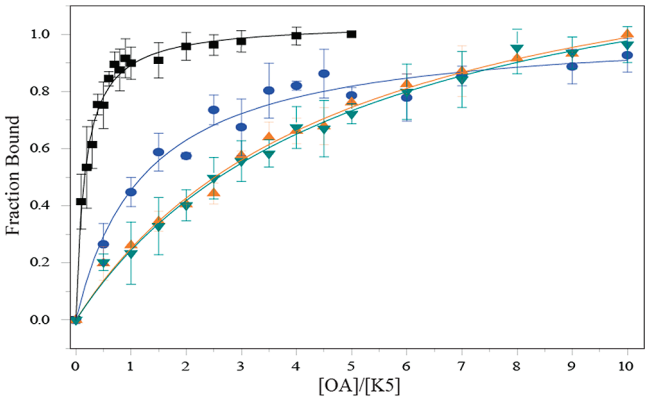

FIGURE 5: Effects of pH and AMCHA on the affinity of kringle 5 for oleic acid: tryptophan fluorescence titration experiments. The fractions of ligand-bound protein are plotted vs the ligand:protein molar ratio [OA]/[K5]. Each titration point is an average of six independent experiments. OA titrations are at pH 5.1 (▲) and pH 7.2 (■) and at 10:1 [AMCHA]/[K5] pH 5.1 (▼) and pH 7.2 (●).

the two protomers as quantitated by the heavy atom RMSD ~ 1.22 Å (vs 0.84 Å overall), which reveals a local conformational "noise" of higher amplitude in the solid state. Indeed, when omitting segment 30−42 from the RMSD calculation, the heavy atom RMSD between the protomers in the crystal decreases from 0.84 to 0.71 Å. Additionally, when deleting this segment and comparing the solution (closest to the mean) NMR structure against the X-ray crystallographic structure of the individual protomers, the backbone RMSD decreases from 0.99 to 0.89 Å and from 0.90 to 0.86 Å for protomers A and B, respectively, which points to a consistent, more pronounced segmental disorder for the 30−42 stretch (Figure 2B). Thus, as demonstrated by both the solution NMR and the crystallographic X-ray structures, we conclude that the dynamic fluctuation, as estimated from the solution NMR $[S^2]_i$ parameter, correlates with intrinsic structural disorder. Moreover, this region of the polypeptide chain varies among kringle domains and is known to affect ligand binding specificity in K1 and K4 (*52*−*55*) and apparently the ligand binding preferences of K5 as well (*51*). For instance, flexibility of the Arg32 side chain may help to stabilize the pose of the carboxylate group of ω-amino acid ligands, such as AMCHA, at the LBS. In this fashion, Arg32 would contribute positive electrostatic potential to the binding site to improve its interaction with the zwitterionic ligand anionic group.

Ligand Binding to Kringle 5. Previous NMR studies have shown that Trp25, His33, Trp62, and Tyr72 are among the amino acid residues most affected by ligand binding to K5 (*11*, *12*, *51*). Thus, Trp25 and Trp62 should afford suitable probes to assess the ligand interaction via intrinsic fluorescence measurements. In order to estimate values of K_a, the equilibrium association constant, the changes in the fluorescence intensity observed upon ligand addition were plotted as a fraction of protein bound vs free ligand concentration and analyzed by nonlinear fit, as described under Materials and Methods.

Consistent with the study of Huet et al. (*8*), we have detected high-affinity interaction between OA and HPgn K5. In order to weaken the effective interaction, ligand binding titrations with OA were performed in the presence of a 10:1 AMCHA/protein molar ratio. As shown in Figure 5, AMCHA decreases the apparent binding affinity of K5 toward OA, consistent with the ligand hindering fatty acid access to the binding site (competitive binding). The K_a of AMCHA (K_a^{AMCHA}) for K5,

and of OA for K5 in the presence of AMCHA ($K_a^{AMCHA+OA}$), were determined, which enabled us to estimate the affinity of the OA for K5. Assuming that OA displaces AMCHA from the binding site, one can estimate the K5 affinity for OA (K_a^{OA}) on the basis of eq 3:

$$K_a^{OA} = K_a^{AMCHA} K_a^{AMCHA+OA} \quad (3)$$

The value obtained at pH 7.2, $K_a^{OA} \sim 2.08 \times 10^4\ mM^{-1}$ ($\equiv 2.08 \times 10^7\ M^{-1}$, corresponding to $K_d^{OA} \sim 47$ nM) is consistent with $K_d^{OA} \sim 58$ nM determined by surface plasmon resonance (*8*). At pH 5.1 negligible AMCHA binding to K5 was detected, while the measured $K_a^{OA} = 50.1 \pm 4.8\ mM^{-1}$. Moreover, within the experimental uncertainties, no difference was found for the OA titration at pH 5.1 whether in the presence ($K_a^{AMCHA+OA} = 45.9 \pm 7.1\ mM^{-1}$) or in the absence ($K_a^{OA} = 50.1 \pm 4.8\ mM^{-1}$) of AMCHA, suggesting that AMCHA has negligible effect on the measured fluorescence changes. Table 2 lists K_a values obtained by fitting the fluorescence data.

Table 2: Kringle 5-Ligand Association Constants (K_a) Determined via Fluorescence Quenching Experiments[a]

	K_a (mM^{-1})		Δ[b]	
ligand	pH 7.2	pH 5.1	pH 7.2	pH 5.1
AMCHA	65.8 ± 6.1		−79.6	
OA		50.1 ± 4.8	−66.1	−16.4
OA (+ AMCHA)[c]	(3.2 ± 0.5) × 10^2	45.9 ± 7.1	−29.8	−19.2

[a]Ligand titrations were performed on 5 μM solutions of K5 dissolved in either 50 mM acetate (pH 5.1) or PBS (pH 7.2) containing 0.05% NaN_3. [b]Fluorescence change (%) obtained from integrating the difference spectrum (±ligand) for the ligand-free protein and the last (highest ligand concentration) titration point. [c]OA titrations were carried out in a 10:1 [AMCHA]/[K5] molar ratio.

Within the pH* 5.1−7.2 range, no significant shift of the $^1H/^{15}N$-HSQC cross-peaks are observed, indicating that the overall structure of the kringle remains unchanged (not shown). Thus, the decreased ligand affinity of ligands at pH* 5.1 is unlikely to stem from structural changes. Therefore, the decreased K_a values probably arise, as is the case for the HPgn K4 (*56*), from a decreased conformational stability (i.e., increased flexibility) of the protein at lower pH values that accompany partial protonation of the imidazole groups of His31 and His33 and of the carboxylate groups in Asp55, Asp57, OA ($pK_a = 5$), and AMCHA ($pK_a = 4.3$).

The K5 Ligand Binding Site. AMCHA- and OA-induced NMR chemical shift perturbations on the K5 were detected via $^1H/^{15}N$-HSQC experiments (Figure 6 and Supporting Information Figure S3), which enabled for the mapping of protein−ligand areas of interaction (Figure 7). In the case of AMCHA, in harmony with what has been found for other ligands (*5*, *10*, *51*), the most affected residues are the anionic pair Asp55/Asp57 as well as His31, His33, and a constellation of aliphatic and aromatic residues comprising Ile35, Phe36, Trp62, Tyr64, Leu71, and Tyr72. $^1H/^{15}N$ chemical shift changes assigned to Gln23, Val58, Gly59, and Gly60 are likely to reflect proximity of these residues, in the periphery of the LBS, to the ligand. OA-induced spectral perturbations involve residues affected by AMCHA including Phe36 (Figures 4C and 7C and Supporting Information Figure S3) in the flexible loop. Thus, for both ligands, the set of perturbed residues include the putative LBS (Figure 7) which leads to the conclusion that both ligands bind at the same site.

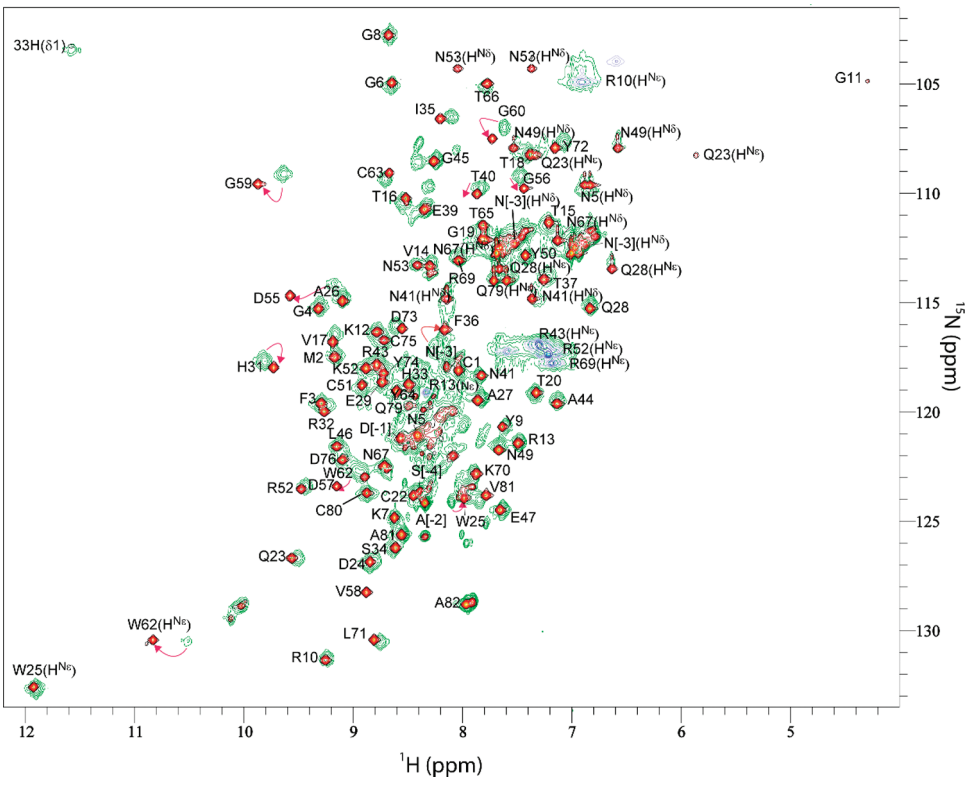

FIGURE 6: Kringle 5 $^1H/^{15}N$ HSQC NMR correlation spectrum: effect of AMCHA binding. Backbone and side-chain amide proton resonances are labeled according to the amino acid type (one-letter code) and sequence numbering. Labels for side-chain resonances (in parentheses) qualify the side-chain amide nitrogen. Green cross-peaks correspond to free kringle 5; red cross-peaks correspond to kringle 5 in the presence of 5:1 ligand/protein molar ratio. Most significant ligand-induced chemical shift perturbations are denoted by magenta arrows. Spectra were recorded at 500 MHz on a 2.2 mM ^{15}N−K5 solution: pH* 5.1, 298 K.

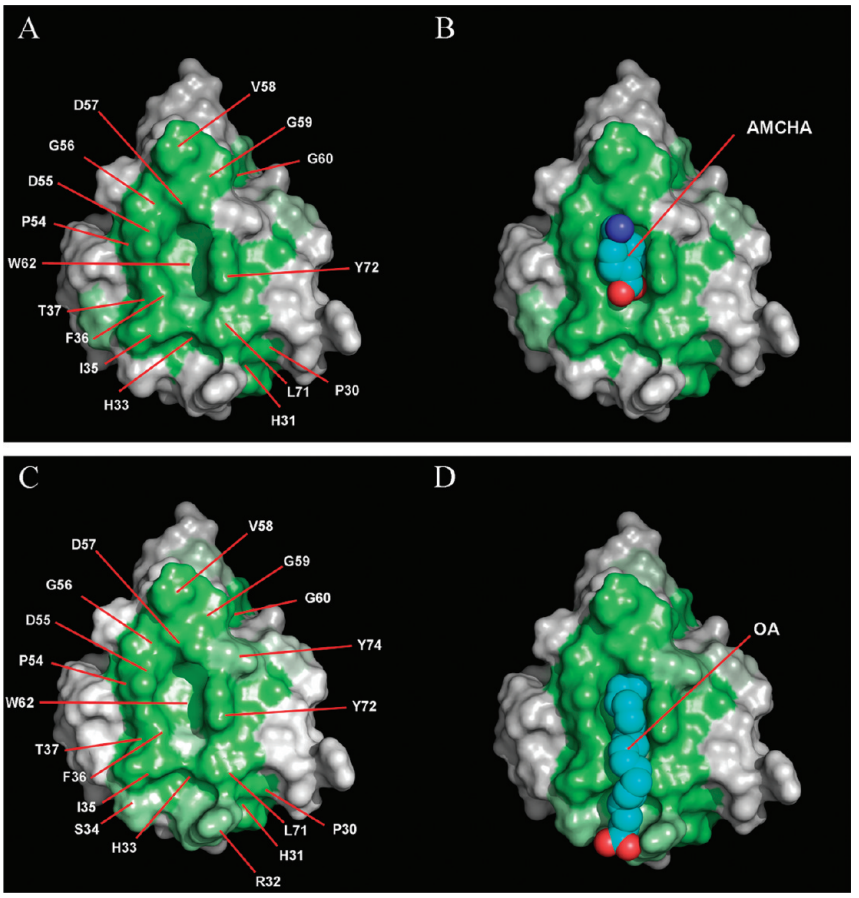

FIGURE 7: Ligand contact surface of kringle 5. Individual residues 1−80 are colored according to a white → green gradient, where the green color intensity is proportional to the amide chemical shift perturbation induced by ligand binding: (A) AMCHA; (C) OA. In (B) and (D), the corresponding ligand atoms are denoted in blue (nitrogen), cyan (carbon), and red (oxygen). Structures of the complexes were obtained using AutoDock4.0 software.

Ligand docking was modeled using the AutoDock4.0 program (*41*−*43*). As indicated by feasibility tests on the HPgn K2−AMCHA complex (see Materials and Methods), when combined with prior knowledge on the binding site location, such as provided by NMR chemical shift perturbation experiments, AutoDock affords a most robust tool for identifying potential ligand interaction site(s) at the protein surface. In the derived model (Figures 7B, 8C, and 9A), AMCHA is shown ion-paired to Asp55 while bridged to the side-chain carboxylate via an H-bond. The generated structure for the AMCHA-K5 complex (Figure 7B) exhibits ∼3.45 Å distance between the K5 Asp55/Asp57 carboxylates' C^{γ} atoms and the ligand N^{ϵ} cationic center. On the other hand, the carboxylate C^{γ} atom of the ligand places itself ∼3.4 Å from the K5 Tyr64 $O^{\eta}H$ group. In other HPgn kringles that bind ω-amino acids, further electrostatic stabilization of the zwitterionic ligand is provided by the Arg71 guanidinium group that ion-pairs the ligand carboxylate group (*57*). In K5 site 71 is occupied by Leu71 which precludes such interaction. However, this is compensated by the ligand carboxylate O atoms H-bonding the Tyr64 hydroxyl group while, by reference to the protein electrostatic surface (Figure 8), the anionic group would become stabilized by a positive potential contributed by residues Gln28, His31, Arg32, and His33 as well as Arg69 and Lys70. By adopting this pose, the ligand cyclohexane group is brought close to the lipophilic side chains of Ile35, Leu71, and Tyr74, as well as of Trp62, sandwiched between the Phe36 and Tyr72 rings (Figure 9A).

Two kringle units dimerize in the crystallographic unit cell (*10*). In the X-ray structures the canonical Asp55/Asp57 interresidue carboxylate $C^{\gamma} \leftrightarrow C^{\gamma}$ average distance is ∼8.15 Å, a configuration nonconducive to bidentate ligand binding (*10*). Upon docking AMCHA to the crystallographic structures the configuration adopted by AMCHA resulted the same for both protomers: the ligand finds minimal energy for the protonated ϵ-amino group lying between the Asp57 and Tyr74 side chains, which are relatively close in space (average $C^{\gamma} \leftrightarrow O^{\eta}$ distance of ∼5 Å between Asp57 and Tyr74, respectively). In the solution structure, however, the ligand places itself between the Asp55/Asp57 side chains whose carboxylate C^{γ} atoms distance themselves by ∼6.23 Å (Figure 10A). As the NMR structure is based on data for the K5−AMCHA complex, it ought to be expected that the Asp55/Asp57 pair orients the two γ-carboxylate groups toward the ligand ϵ-ammonium group, in a fashion that differs from the one predicted for the "frozen" crystallographic structure, solved in the absence of ligand (Figure 10B). While it has been shown that the topologies of the kringles' lysine binding sites (LBSs) are preformed (*10*, *58*), our study suggests that a degree of structural flexibility manifests itself in order to accommodate the ligand at the LBS.

For the sake of comparison between OA and AMCHA, the structures of minimum energies are shown for each of the two ligands in Figures 7−9. In the case of AMCHA, only one (lowest energy) conformation was found. In contrast, as shown in Figure 11A, OA is likely to adopt various conformations upon docking.

K5-docked OA structures (Figure 7D) were screened on the basis of consistency with the experimental ligand-induced chemical shift perturbations (Figure 7C and Supporting Information

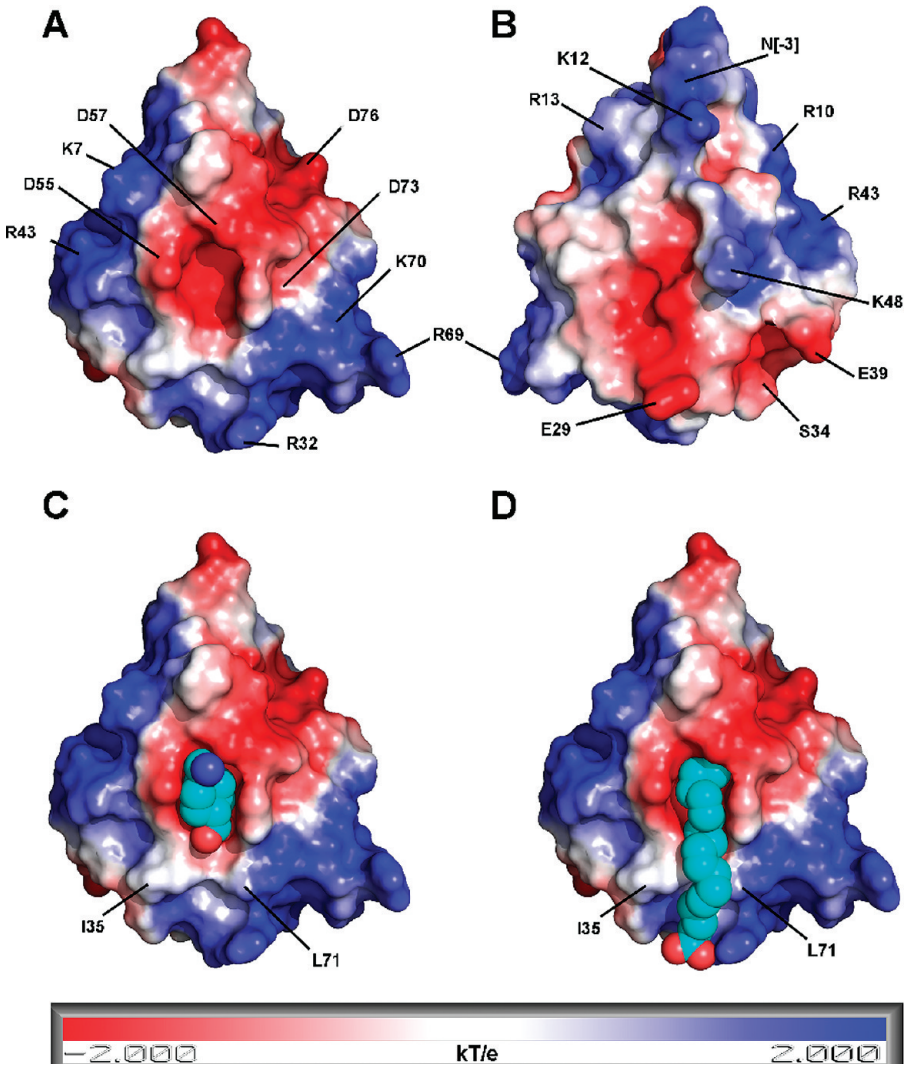

FIGURE 8: Kringle 5 surface electrostatic potential. Areas of neutral, negative, and positive potential are depicted in white, red, and blue, respectively, corresponding to a gradient from −2 (red) to +2 (blue) kT/e, where k is the Boltzmann constant, T is the temperature, and e is the electron charge. (A), (C), and (D) front views; (B) back view; (C) K5-AMCHA complex; (D) K5−OA complex. Ligand atoms are color-coded as in Figure 7. Charged residues are labeled in (A) and (B) according to one-letter amino acid code. Key hydrophobic residues Ile35 and Leu71 are indicated in (C) and (D). Electrostatic surface was calculated using Apbs 1.1 plug-in for Pymol (*63*).

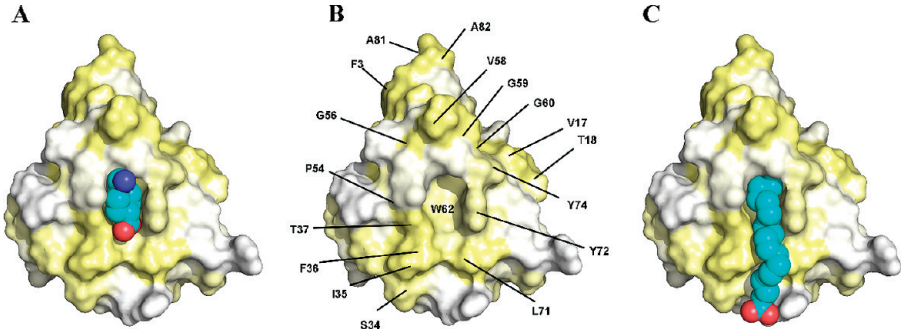

FIGURE 9: Kringle 5 solution structure showing the LBS hydrophobic groove centered at Trp62: front view. Lipophilic character is depicted in a white → yellow gradient, where the yellow color intensity is proportional to the residue lipophilicity (*64*). (A) K5−AMCHA complex; (B) ligand-free kringle 5; (C) K5−OA complex. Ligand atoms are color-coded as in Figure 7. AutoDock4.0 software was used for ligand docking.

Figure S3). The OA model shows the ligand C11−C18 stretch to be narrowly restricted to a rather defined conformation (Figure 11A) while the C1−C10 stretch that ends at the carboxylate group orients itself toward the flexible Pro30-His31-Arg32-His33-Ser34-Ile35 K5 segment. Thus, the C1−C10 stretch is suggested to be less constrained, to the extent of originating two divergent conformations, like the branches of a Y, each considerably more diffuse than the stem within the binding site hydrophobic groove (Figure 11A). Noteworthy, the model (Figure 9C) places the C9−C10 *cis* double bond in close proximity to the aromatic rings of Trp62 and Tyr72 while restrained laterally by the lipophilic side chains of Ile35, Phe36,

and Leu71. According to this view, the Ile35/Leu71 pair defines a sort of molecular "ice tong" that clamps the OA chain at the C11−C12 locus, next to the C9−C10 double bond (Figures 7D, 8D, and 9C). This device would stabilize the pose of the ligand C11-C18 "stem" within the binding site groove structured by the side chains of residues Ile35, Phe36, Trp62, Tyr72, and Leu71.

In the analysis above, the ligands were allowed flexibility while the protein was treated as a rigid molecule. In contrast, AutoDock dynamic runs that allow for the K5 Arg32 side chain to be flexible confirm that while the C11−C18 stretch of OA remains locked within the hydrophobic pocket, the conformation at the carboxylate end is modulated by the positioning of the Arg32 cationic guanidinium group (Figure 11B,C). The aliphatic side chain of the Leu71 residue expands the hydrophobic surface by extending the LBS's hydrophobic cleft, conceivably enhancing the pose of the OA hydrocarbon component while, in parallel, the His31-Arg32-His33 stretch contributes positive electrostatic potential, thus contributing stability to the pose of the OA carboxylate group.

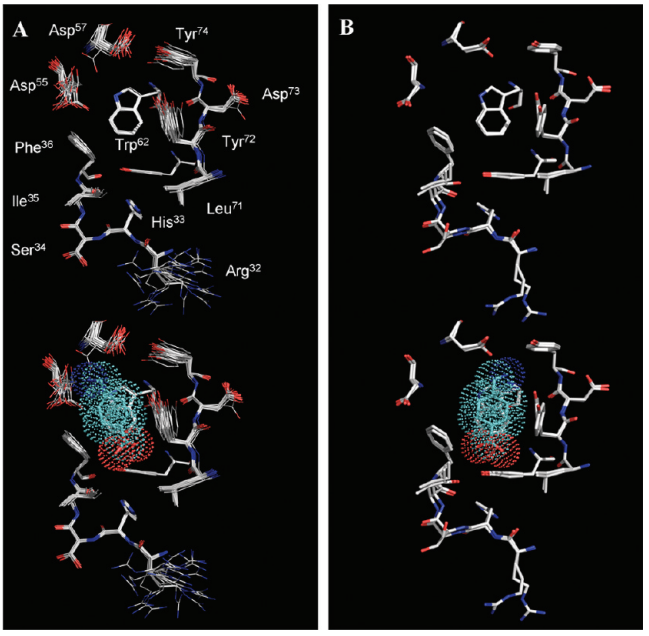

FIGURE 10: Kringle 5 binding site AMCHA-docked structures and the X-ray crystallographic structure. (A) Selected NMR ensemble of 20 kringle 5 structures: ligand-free (top); complexed with AMCHA (bottom). (B) Overlapped LBS residues for the two structures of kringle 5 solved by X-ray crystallography (*10*): ligand-free (top); complexed with AMCHA (bottom). Protein is in stick heavy atom representation; ligand atoms are color-coded as in Figure 7.

We have suggested (*51*) that ammonium or guanidinium groups, present in arginine or benzamidine ligands, are not the primary determinants of ligand affinity toward K5 and that it is the hydrophobic interactions that stabilize the protein−ligand complex. Consistent with this hypothesis, the interaction between the OA molecule with the LBS hydrophobic side chains would afford the key factor stabilizing the OA−K5 complex, while the electrostatic pairing of the His31-Arg32-His33 stretch with the ligand carboxylate group adds a degree of dynamic flexibility to the resulting structure.

CONCLUSIONS

NMR analysis points to AMCHA-bound K5 having a compact fold in solution, consistent with preliminary studies (*11*, *12*, *51*) and the crystallographic model for the apoprotein (*10*). The AMCHA binding site of K5 comprises the anionic pair Asp55/Asp57 and an area lined by a constellation of aliphatic and aromatic side chains attached to residues His31, His33, Ile35, Phe36, Trp62, Tyr64, Leu71, and Tyr72.

The same region of the domain interacts with OA; however, the $K_a \sim 2.08 \times 10^4\ mM^{-1}$ estimated for OA is significantly larger than $K_a \sim 65.8\ mM^{-1}$ for AMCHA, indicating a tighter interaction with the fatty acid. The preference for OA vis-à-vis small zwitterionic ligands may be rationalized on the basis of an expanded hydrophobic surface exposed by the K5 binding site, as it includes Ile35 and Leu71, that interacts with the C11−C18 stretch of OA (Figure 11A). When Leu71 is replaced by Arg71, as found in K1, K2, and K4, the binding specificity switches to ω-amino acid as well as short carboxylic acid ligands (*10*). This may relate to the observation that, among the Pgn kringles, K5 is the most potent inhibitor of cell proliferation and cell migration (*59*, *60*).

Thus, although the HPgn K5 shares 50% sequence identity and a similar fold with the other four kringle domains in HPgn, its ligand binding properties (*5*, *51*) are quite distinct. For example, K5 affinities for benzamidine and benzylamine ($K_a \sim 3.4$ and

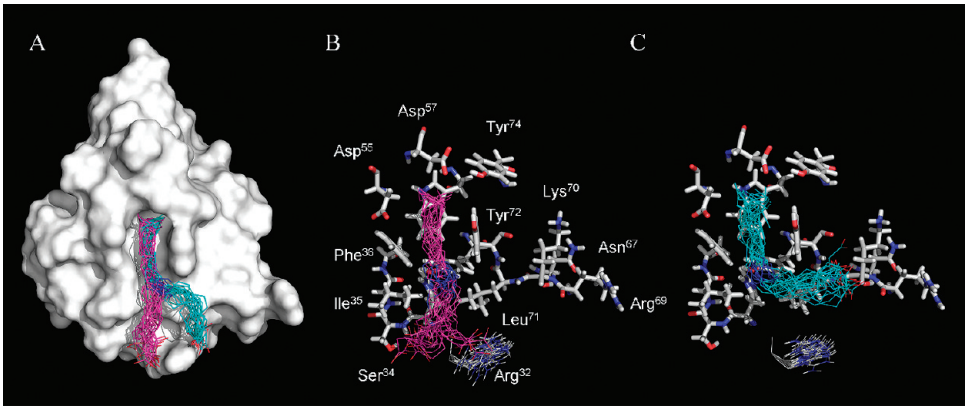

FIGURE 11: Solution structure of kringle 5 complexed with oleic acid. Two different subsets of 23 possible OA structures are shown. (A) Surface representation of the OA-docked kringle 5 structures obtained with the protein rigid. (B, C) Expansion of the K5−OA interacting surface with two different subsets of 23 OA docked structures; the structures were obtained by allowing flexibility for the Arg32 side chain during the docking. OA chains are colored magenta for those conformations with the higher docking energy (B) and cyan for those with lower energy (C). The ligand *cis* double bond is colored blue, oxygen atoms are in red, and nitrogen atoms in blue. Bound OA is shown in thin stick representation; the kringle binding site structure expansion (B, C) is shown in thick stick representation. OA structures were obtained via AutoDock4.0.

6.3 mM^{-1}, respectively) are 1 order of magnitude higher than the corresponding affinities of K1, K2, and K4 for the same ligands (K3 does not measurably interact with either ligand).

Because lysyl compounds exhibit weak binding to kringle domains ($K_d \sim 42 \times 10^4$ μM (*5*)), the interaction with lysine side chains exposed by the fibrin meshwork would enable the protein to adhere to the clot while "crawling" through the fibrin meshwork in a dynamic fashion, as the individual, in tandem, kringle modules are in on/off equilibrium between bound and unbound states (*51*). Hence, it is suggested that, upon binding to K5, OA might exert an inhibitory effect on fibrin binding. This would result in Plm activity being affected, as OA occupancy of the K5 binding site would interfere with the domain adhering to the fibrin polymer, consistent with the reported *in vitro* OA inhibition of Plm activity (*6*, *8*, *9*). However, the effect of OA binding to K5 is unlikely to fully account for its inhibitory effect on Plm. Indeed, it has been proposed that the K5 domain intramolecularly interacts with the N-terminal preactivation peptide, thus resulting in a "closed" Pgn conformation (*61*, *62*). From this standpoint, OA binding to the domain would favor the open conformation of Pgn which, in turn, would facilitate its activation to Plm.

Since the overall Pgn affinity for fibrin results of multiple kringle-mediated binding interactions, a more extensive study of fatty acid binding to individual kringle domains and multikringle Pgn fragments is in order. It is our hope that the description of the K5−OA interaction presented in this paper provides a basis for an improved understanding of the molecular mechanisms of Pgn-mediated fatty acid regulation of fibrinolysis, as well as cell proliferation and migration in the extracellular matrix.

ACKNOWLEDGMENT

NMR experiments were run at the CMU Biomolecular and CMU Chemistry Department NMR facilities. The latter is supported, in part, by NSF Grant CHE-0130903. NMR data on the ^{15}N-labeled protein were recorded, in part, by L. G. Barrientos. The authors thank V. Simplaceanu and R. Gil for expert NMR assistance and B. Armitage for access to fluorescence spectrophotometers.

SUPPORTING INFORMATION AVAILABLE

Three additional figures as described in the text. This material is available free of charge via the Internet at http://pubs.acs.org.

REFERENCES

1. Sottrup-Jensen, L., Claeys, H., Zajdel, M., Petersen, T. E., and Magnusson, S. (1978) The primary structure of human plasminogen: isolation of two lysine-binding fragments and one "mini-"plasminogen (mw, 38,000) by elastase-catalyzed-specific limited proteolysis. *Prog. Chem. Fibrinolysis Thrombolysis 3*, 191–209.
2. Schaller, J., Gerber, S., Kämpfer, U., Lejon, S., and Trachsel, C. (2008) Human blood plasma proteins: structure and function, John Wiley & Sons, Chichester, West Sussex, England, and Hoboken, NJ.
3. Park, C. H., and Tulinsky, A. (1986) 3-dimensional structure of the kringle sequence: structure of prothrombin fragment-1. *Biochemistry 25*, 3977–3982.
4. Gehrmann, M., Briknarova, K., Bányai, L., Patthy, L., and Llinás, M. (2002) The col-1 module of human matrix metalloproteinase-2 (MMP-2): structural/functional relatedness between gelatin-binding fibronectin type II modules and lysine-binding kringle domains. *Biol. Chem. 383*, 137–148.
5. Marti, D. N., Hu, C. K., An, S. S. A., vonHaller, P., Schaller, J., and Llinás, M. (1997) Ligand preferences of kringle 2 and homologous domains of human plasminogen: canvassing weak, intermediate, and high-affinity binding sites by ^{1}H-NMR. *Biochemistry 36*, 11591–11604.
6. Higazi, A. A., Aziza, R., Samara, A. A., and Mayer, M. (1994) Regulation of fibrinolysis by nonesterified fatty acids. *Biochem. J. 300*, 251–255.
7. Higazi, A. A., Barghouti, I. I., Ayesh, S. K., Mayer, M., and Matzner, Y. (1994) Inhibition of neutrophil activation by fibrinogen. *Inflammation 18*, 525–535.
8. Huet, E., Cauchard, J. H., Berton, A., Robinet, A., Decarme, M., Hornebeck, W., and Bellon, G. (2004) Inhibition of plasmin-mediated prostromelysin-1 activation by interaction of long chain unsaturated fatty acids with kringle 5. *Biochem. Pharmacol. 67*, 1011–1011.
9. Rabai, G., Varadi, B., Longstaff, C., Sotonyi, P., Kristof, V., Timar, F., Machovich, R., and Kolev, K. (2007) Fibrinolysis in a lipid environment: modulation through release of free fatty acids. *J. Thromb. Haemostasis 5*, 1265–1273.
10. Chang, Y., Mochalkin, I., McCance, S. G., Cheng, B. S., Tulinsky, A., and Castellino, F. J. (1998) Structure and ligand binding determinants of the recombinant kringle 5 domain of human plasminogen. *Biochemistry 37*, 3258–3271.
11. Thewes, T., Ramesh, V., Simplaceanu, E. L., and Llinás, M. (1987) Isolation, purification and ^{1}H-NMR characterization of a kringle 5 domain fragment from human plasminogen. *Biochim. Biophys. Acta 912*, 254–269.
12. Thewes, T., Ramesh, V., Simplaceanu, E. L., and Llinás, M. (1988) Analysis of the aromatic ^{1}H-NMR spectrum of the kringle 5 domain from human plasminogen: evidence for a conserved kringle fold. *Eur. J. Biochem. 175*, 237–249.
13. Zajicek, J., Chang, Y., and Castellino, F. J. (2000) The effects of ligand binding on the backbone dynamics of the kringle 1 domain of human plasminogen. *J. Mol. Biol. 301*, 333–347.
14. Sreerama, N., and Woody, R. W. (2000) Estimation of protein secondary structure from circular dichroism spectra: Comparison of CONTIN, SELCON, and CDSSTR methods with an expanded reference set. *Anal. Biochem. 287*, 252–260.
15. Cao, Y. H., Chen, A., An, S. S. A., Ji, R. W. D., Davidson, D., Cao, Y. M., and Llinás, M. (1997) Kringle 5 of plasminogen is a novel inhibitor of endothelial cell growth. *J. Biol. Chem. 272*, 22924–22928.
16. Delaglio, F., Grzesiek, S., Vuister, G. W., Zhu, G., Pfeifer, J., and Bax, A. (1995) Nmrpipe: a multidimensional spectral processing system based on unix pipes. *J. Biomol. NMR 6*, 277–293.
17. Vranken, W. F., Boucher, W., Stevens, T. J., Fogh, R. H., Pajon, A., Llinás, P., Ulrich, E. L., Markley, J. L., Ionides, J., and Laue, E. D. (2005) The CCPN data model for NMR spectroscopy: development of a software pipeline. *Proteins: Struct., Funct., Bioinf. 59*, 687–696.
18. Demarco, A. (1977) pH-dependence of internal references. *J. Magn. Reson. 26*, 527–528.
19. Live, D. H., Davis, D. G., Agosta, W. C., and Cowburn, D. (1984) Long-range hydrogen-bond mediated effects in peptides: ^{15}N NMR study of gramicidin-S in water and organic-solvents. *J. Am. Chem. Soc. 106*, 1939–1941.
20. Vuister, G. W., and Bax, A. (1993) Quantitative J correlation: a new approach for measuring homonuclear 3-bond $J(H^NH^\alpha)$ coupling constants in ^{15}N-enriched proteins. *J. Am. Chem. Soc. 115*, 7772–7777.
21. Grishaev, A., and Llinás, M. (2004) BACUS: A Bayesian protocol for the identification of protein NOESY spectra via unassigned spin systems. *J. Biomol. NMR 28*, 1–10.
22. Grishaev, A., Steren, C. A., Wu, B., Pineda-Lucena, A., Arrowsmith, C., and Llinás, M. (2005) ABACUS, a direct method for protein NMR structure computation via assembly of fragments. *Proteins: Struct., Funct., Bioinf. 61*, 36–43.
23. Ozhogina, O. A., Grishaev, A., Bominaar, E. L., Patthy, L., Trexler, M., and Llinás, M. (2008) NMR solution structure of the neurotrypsin kringle domain. *Biochemistry 47*, 12290–12298.
24. Grishaev, A., and Bax, A. (2004) An empirical backbone-backbone hydrogen-bonding potential in proteins and its applications to NMR structure refinement and validation. *J. Am. Chem. Soc. 126*, 7281–7292.
25. Rieping, W., Habeck, M., Bardiaux, B., Bernard, A., Malliavin, T. E., and Nilges, M. (2007) ARIA2: automated NOE assignment and data integration in NMR structure calculation. *Bioinformatics 23*, 381–382.
26. Laskowski, R. A., Rullmann, J. A. C., MacArthur, M. W., Kaptein, R., and Thornton, J. M. (1996) AQUA and PROCHECK-NMR: programs for checking the quality of protein structures solved by NMR. *J. Biomol. NMR 8*, 477–486.
27. Doreleijers, J. F., Rullmann, J. A. C., and Kaptein, R. (1998) Quality assessment of NMR structures: a statistical survey. *J. Mol. Biol. 281*, 149–164.

28. Doreleijers, J. F., Raves, M. L., Rullmann, T., and Kaptein, R. (1999) Completeness of NOEs in protein structures: a statistical analysis of NMR data. *J. Biomol. NMR 14*, 123–132.
29. Kabsch, W., and Sander, C. (1983) Dictionary of protein secondary structure: pattern-recognition of hydrogen-bonded and geometrical features. *Biopolymers 22*, 2577–2637.
30. Heinig, M., and Frishman, D. (2004) STRIDE: a web server for secondary structure assignment from known atomic coordinates of proteins. *Nucleic Acids Res. 32*, W500–W502.
31. King, S. M., and Johnson, W. C. (1999) Assigning secondary structure from protein coordinate data. *Proteins: Struct., Funct., Genet. 35*, 313–320.
32. Farrow, N. A., Zhang, O. W., Formankay, J. D., and Kay, L. E. (1995) Comparison of the backbone dynamics of a folded and an unfolded Sh3 domain existing in equilibrium in aqueous buffer. *Biochemistry 34*, 868–878.
33. Grzesiek, S., and Bax, A. (1993) The importance of not saturating H_2O in protein NMR: application to sensitivity enhancement and NOE measurements. *J. Am. Chem. Soc. 115*, 12593–12594.
34. Lipari, G., and Szábo, A. (1982) Model-free approach to the interpretation of nuclear magnetic-resonance relaxation in macromolecules. 1. Theory and range of validity. *J. Am. Chem. Soc. 104*, 4546–4559.
35. Lipari, G., and Szábo, A. (1982) Model-free approach to the interpretation of nuclear magnetic-resonance relaxation in macromolecules. 2. Analysis of experimental results. *J. Am. Chem. Soc. 104*, 4559–4570.
36. Mandel, A. M., Akke, M., and Palmer, A. G. (1995) Backbone dynamics of *Escherichia coli* ribonuclease H_1: correlations with structure and function in an active enzyme. *J. Cell. Biochem.,* 29–29.
37. Kay, L. E., Torchia, D. A., and Bax, A. (1989) Backbone dynamics of proteins as studied by ^{15}N inverse detected heteronuclear NMR-spectroscopy: application to staphylococcal nuclease. *Biochemistry 28*, 8972–8979.
38. Shuker, S. B., Hajduk, P. J., Meadows, R. P., and Fesik, S. W. (1996) Discovering high-affinity ligands for proteins: SAR by NMR. *Science 274*, 1531–1534.
39. Petros, A. M., Ramesh, V., and Llinás, M. (1989) ^{1}H-NMR studies of aliphatic ligand-binding to human plasminogen kringle 4. *Biochemistry 28*, 1368–1376.
40. Kawamura, T., Le, L. U. K., Zhou, H. J., and Dahlquist, F. W. (2007) Solution structure of *Escherichia coli* PapI, a key regulator of the pap pili phase variation. *J. Mol. Biol. 365*, 1130–1142.
41. Goodsell, D. S., and Olson, A. J. (1990) Automated docking of substrates to proteins by simulated annealing. *Proteins: Struct., Funct., Genet. 8*, 195–202.
42. Morris, G. M., Goodsell, D. S., Halliday, R. S., Huey, R., Hart, W. E., Belew, R. K., and Olson, A. J. (1998) Automated docking using a Lamarckian genetic algorithm and an empirical binding free energy function. *J. Comput. Chem. 19*, 1639–1662.
43. Goodsell, D. S., Morris, G. M., and Olson, A. J. (1996) Automated docking of flexible ligands: applications of AutoDock. *J. Mol. Recognit. 9*, 1–5.
44. Marti, D. N., Schaller, J., and Llinás, M. (1999) Solution structure and dynamics of the plasminogen kringle 2-AMCHA complex: 3(1)-helix in homologous domains. *Biochemistry 38*, 15741–15755.
45. Rejante, M. R., and Llinás, M. (1994) Solution structure of the epsilon-aminohexanoic acid complex of human plasminogen kringle-1. *Eur. J. Biochem. 221*, 939–949.
46. Mathews, I. I., VanderhoffHanaver, P., Castellino, F. J., and Tulinsky, A. (1996) Crystal structures of the recombinant kringle 1 domain of human plasminogen in complexes with the ligands epsilon-aminocaproic acid and trans-4-(aminomethyl)cyclohexane-1-carboxylic acid. *Biochemistry 35*, 2567–2576.
47. Wu, T. P., Padmanabhan, K., Tulinsky, A., and Mulichak, A. M. (1991) The refined structure of the epsilon-aminocaproic acid complex of human plasminogen kringle 4. *Biochemistry 30*, 10589–10594.
48. Hansen, A. P., Petros, A. M., Meadows, R. P., Nettesheim, D. G., Mazar, A. P., Olejniczak, E. T., Xu, R. X., Pederson, T. M., Henkin, J., and Fesik, S. W. (1994) Solution structure of the amino-terminal fragment of urokinase-type plasminogen activator. *Biochemistry 33*, 4847–4864.
49. Chitayat, S., Kanelis, V., Koschinsky, M. L., and Smith, S. P. (2007) Nuclear magnetic resonance (NMR) solution structure, dynamics, and binding properties of the kringle IV type 8 module of apolipoprotein(a). *Biochemistry 46*, 1732–1742.
50. Maciejewski, M. W., Liu, D. J., Prasad, R., Wilson, S. H., and Mullen, G. P. (2000) Backbone dynamics and refined solution structure of the N-terminal domain of DNA polymerase beta. Correlation with DNA binding and dRP lyase activity. *J. Mol. Biol. 296*, 229–253.
51. Thewes, T., Constantine, K., Byeon, I. J. L., and Llinás, M. (1990) Ligand interactions with the kringle 5 domain of plasminogen: a study by ^{1}H-NMR spectroscopy. *J. Biol. Chem. 265*, 3906–3915.
52. Lerch, P. G., and Rickli, E. E. (1980) Investigations on the identification and localization of lysine binding sites of human plasminogen. *Protides Biol. Fluids 28*, 371–374.
53. Winn, E. S., Hu, S. P., Hochschwender, S. M., and Laursen, R. A. (1980) Studies on the lysine binding sites of human plasminogen: the effect of ligand structure on the binding of lysine analogs to plasminogen. *Eur. J. Biochem. 104*, 579–586.
54. Demarco, A., Hochschwender, S. M., Laursen, R. A., and Llinás, M. (1982) Human plasminogen: Proton NMR-studies on kringle-1. *J. Biol. Chem. 257*, 2716–2721.
55. Petros, A. M., Ramesh, V., and Llinás, M. (1989) ^{1}H-NMR studies of aliphatic ligand binding to human plasminogen kringle 4. *Biochemistry 28*, 1368–1376.
56. Demarco, A., Motta, A., Llinás, M., and Laursen, R. A. (1985) Macro-stabilities and micro-stabilities of the kringle 4 domain from plasminogen: the effect of ligand binding. *Biophys. J. 48*, 411–422.
57. Váli, Z., and Patthy, L. (1980) Essential carboxyl group and guanidino-group in the lysine binding site of human plasminogen. *Biochem. Biophys. Res. Commun. 96*, 1804–1811.
58. Ramesh, V., Petros, A. M., Llinás, M., Tulinsky, A., and Park, C. H. (1987) Proton magnetic-resonance study of lysine-binding to the kringle 4 domain of human plasminogen: the structure of the binding-site. *J. Mol. Biol. 198*, 481–498.
59. Lu, H., Dhanabal, M., Volk, R., Waterman, M. J. F., Ramchandran, R., Knebelmann, B., Segal, M., and Sukhatme, V. P. (1999) Kringle 5 causes cell cycle arrest and apoptosis of endothelial cells. *Biochem. Biophys. Res. Commun. 258*, 668–673.
60. Ji, W. R., Barrientos, L. G., Llinás, M., Gray, H., Villarreal, X., DeFord, M. E., Castellino, F. J., Kramer, R. A., and Trail, P. A. (1998) Selective inhibition by kringle 5 of human plasminogen on endothelial cell migration, an important process in angiogenesis. *Biochem. Biophys. Res. Commun. 247*, 414–419.
61. An, S. S. A., Carreño, C., Marti, D. N., Schaller, J., Albericio, F., and Llinás, M. (1998) Lysine-50 is a likely site for anchoring the plasminogen N-terminal peptide to lysine-binding kringles. *Protein Sci. 7*, 1960–1969.
62. Marshall, J. M., Brown, A. J., and Ponting, C. P. (1994) Conformational studies of human plasminogen and plasminogen fragments: evidence for a novel 3rd conformation of plasminogen. *Biochemistry 33*, 3599–3606.
63. Baker, N. A., Sept, D., Joseph, S., Holst, M. J., and McCammon, J. A. (2001) Electrostatics of nanosystems: application to microtubules and the ribosome. *Proc. Natl. Acad. Sci. U.S.A. 98*, 10037–10041.
64. Hessa, T., Kim, H., Bihlmaier, K., Lundin, C., Boekel, J., Andersson, H., Nilsson, I., White, S. H., and von Heijne, G. (2005) Recognition of transmembrane helices by the endoplasmic reticulum translocon. *Nature 433*, 377–381.